JOURNAL OF GEOPHYSICAL RESEARCH, VOL. 114, A12309, doi:10.1029/2009JA014175, 2009

A study of the Weddell Sea Anomaly observed by FORMOSAT-3/COSMIC

Maosheng He,[1,2] Libo Liu,[1] Weixing Wan,[1] Baiqi Ning,[1] Biqiang Zhao,[1] Jin Wen,[1,2] Xin'an Yue,[1] and Huijun Le[1]

Received 19 February 2009; revised 12 July 2009; accepted 14 August 2009; published 9 December 2009.

[1] More than two years of COSMIC electron density profiles at low solar activities are collected to study the evolution of the Weddell Sea Anomaly (WSA), which appears as an evening enhancement in electron density during local summer. Observations show that the change in NmF2 (the F2 peak electron density) is associated with the change in hmF2 (the F2 peak height), while the latter is correlated closely with the components of the geomagnetic field. We find that (1) in the afternoon, hmF2 is more liable to rise drastically in regions with a larger $|\sin(2I)|$ value, which would occur early at certain declinations, eastward in the southern hemisphere and westward in the northern hemisphere; (2) subsequently, a larger increment of hmF2 is coincidentally followed by a stronger enhancement of NmF2 and the enhancement ends just around the local sunset; and (3) in midlatitudes, the evolution pattern of hmF2 in the evening of equinoxes and winter is similar to that in summer, albeit without a lasting NmF2 enhancement as that in summer. These features suggest that the NmF2 enhancement and the hmF2 increase could arise from the thermospheric wind effect, and solar photoionization plays a crucial role in the enhancement as well. The general midlatitude F2 layer enhancement in local summer evening is consistent with the WSA on the above features, indicating that the WSA is a manifestation, with a particular geometry of the magnetic field, of the evening enhancement induced by the winds.

Citation: He, M., L. Liu, W. Wan, B. Ning, B. Zhao, J. Wen, X. Yue, and H. Le (2009), A study of the Weddell Sea Anomaly observed by FORMOSAT-3/COSMIC, *J. Geophys. Res.*, *114*, A12309, doi:10.1029/2009JA014175.

1. Introduction

[2] On the east of the Antarctic Peninsula, the diurnal maximum of ionospheric electron density occurs in the evening or at night in local summer. *Bellchambers and Piggott* [1958] first recorded this phenomenon at Halley Bay (76°S, 26°W, dip −64.6°, apex latitude −62.2°). By analyzing ionospheric data from ionosondes widespread in the Antarctic, *Penndorf* [1965] found that the diurnal maximum of foF2 (critical frequency of the F2 layer, proportional to the square root of the peak electron density, NmF2) occurs at 04 UT from the Falkland Islands (52°S, 60°W, dip −50.4°, apex latitude −38.1°) to the southern shore of the Weddell Sea (around 75°S, 30°W, dip −64°, apex latitude −61°). It implies that the diurnal maximum NmF2 occurs at 00–02 LT over there, which is quite different from the typical daytime maximum in the diurnal variation of NmF2. Accordingly, *Penndorf* [1965] named it Weddell Sea Anomaly (WSA). The WSA is a prominent feature of the summer southern ionosphere, presenting close associations with other essential features of the ionosphere, e.g., the heavy-ion stagnation trough and the plasmapause [*Horvath and Lovell*, 2009a, 2009b].

[3] Many studies have documented that this unusual evening electron density enhancement is not specifically confined to the summer Weddell Sea zone. In the summer southern hemisphere, the electron density enhancement covers a much larger area than *Penndorf*'s [1965] report. Across the southeastern Pacific and southwestern Atlantic Ocean, the diurnal maximum of total electron content (TEC) appears at 22–24 LT [*Horvath and Essex*, 2003; *Horvath*, 2006]. NmF2 increases in the summer evening over a wider range of longitudes where the magnetic dip equator offsets southward away from the geographic equator [*Burns et al.*, 2008]. In addition, such an electron enhancement also occurs in the summer northern hemisphere. It is widely observed with various techniques that the typical diurnal variation of NmF2 is insignificant in summer northern midlatitudes, where the electron density usually increases and reaches its diurnal maximum in the evening. [e.g., *Chan and Colin*, 1969; *Ivanov-Kholodny and Mikhailov*, 1986; *H. Liu et al.*, 2007; *Rishbeth and Kervin*, 1968; *Rishbeth and Mendillo*, 2001]. The evening enhancement in the northern hemisphere shares a common feature with that in the southern hemisphere; that is, the enhancement is most prominent in longitude sectors where

[1]Beijing National Observatory of Space Environment, Institute of Geology and Geophysics, Chinese Academy of Sciences, Beijing, China.
[2]Graduate University of Chinese Academy of Sciences, Beijing, China.

0148-0227/09/2009JA014175$09.00

the dip equator excurses farthest toward the geographic pole [*Lin et al.*, 2009; *Horvath and Lovell*, 2009b]. In this study, all the above midlatitude enhancements, appearing in the longitude sectors where the dip equator shifts toward the pole in the both hemispheres, are termed the general Weddell Sea Anomaly (general WSA) as a distinction from Penndorf-defined WSA (called special WSA hereinafter).

[4] A relevant simulation carried out first by *Rishbeth* [1967, 1968] showed that, at summer dusk, NmF2 tends to increase at midlatitudes, which was explained as follows. The equatorward wind prevails at nighttime, which could drive the plasma to drift upward; in summer, local sunset occurs later; once the drift becomes upward before the solar photoionization ceases, the plasma is pushed to higher altitudes where the recombination is very slow; then, NmF2 could increase and plasma would be preserved for a longer time. Based on these results, *Dudeney and Piggott* [1978] proposed the thermospheric wind mechanism which ascribes the WSA to the interplay of solar photoionization, thermospheric winds and the pattern of the magnetic field.

[5] The wind mechanism is consistent with a lot of observations. With ionosonde observations, *Rastogi* [1960] found that the midnight foF2 in the southern hemisphere was regulated more by the dip angle than by the geographic or geomagnetic latitude, especially around December solstice. TOPEX TEC maps illustrated the connection between the magnetic declination and the WSA: the western boundary of the WSA is limited by contours of magnetic declination [*Horvath*, 2006]. In the study about the storm on January 10, 1997, *Horvath* [2007] pointed out that the thermospheric wind is one of the most important factors that modify the WSA.

[6] However, there are still several other potential mechanisms, including the transportation of plasma from the dayside ionosphere, the downward flux from the plasmasphere, and so on. Using COSMIC data, *Burns et al.* [2008] studied the ionosphere over the South Pacific at summer dusk and discussed characteristics of various mechanisms about the WSA in detail. They pointed out that the winds would not be significant at driving electrons upward along the field lines, if the zonal wind prevails there around dusk. As revealed by the theoretical model [*Dickinson et al.*, 1981], the winds are mainly zonal at dusk in general.

[7] The main objective of this paper is to employ the huge number of electron density profiles, retrieved from FORMOSAT-3/COSMIC (F3/C, for short) observations, to study the evolution of F2 peak parameters (NmF2 and hmF2) as well as their longitudinal, seasonal variability in regions where both the general WSA and the special WSA appear. In this paper, the evening evolution of global NmF2 in different seasons is investigated in UT maps (section 3.1) and LT maps (section 3.2), then the connection between the increases of hmF2 and NmF2 as well as their connections with components of the magnetic field are explored (sections 3.2 and 3.3), and then potential mechanisms are discussed in detail (sections 4.1 and 4.2). Finally, a case study of the evening evolution of hourly increment of NmF2 in the southern summer is conducted (section 4.3).

2. Data

[8] The F3/C (Constellation Observing System for Meteorology, Ionosphere, and Climate mission, also called FORMOSAT-3) mission consists of six microsatellites. Each of them records approximately 500 occultation events per day. One electron density profile of the ionosphere could be derived per occultation event [cf. *Lei et al.*, 2007b; *Rocken et al.*, 2000; *Schreiner et al.*, 2007]. Preliminary validations of the data have been done by *Lei et al.* [2007b] and *Schreiner et al.* [2007]. *Lei et al.* [2007b] showed a good agreement between F3/C profiles and data from incoherent scatter radars and ionosondes. Several studies also showed the consistent climatology between observations by IRO (ionospheric radio occultation) and traditional techniques [e.g., *Luan and Solomon*, 2008] and potential values of IRO in ionospheric climatology studies as well [e.g., *Lin et al.*, 2009; *Liu et al.*, 2008, 2009; *Zeng et al.*, 2008].

[9] The electron density profiles used for this investigation are postprocessed F3/C data obtained from the COSMIC Data Analysis and Archive Center. We used the data within the period from day of year (DOY) 121, 2006 to DOY 213, 2008, when the level of solar activity is at its minimum. As shown by *Liu et al.* [2008, Figure 2], the F3/C electron density profiles exhibit a good quality of favorable uniformities in space and time.

[10] We fit each density profile at altitude between 160 and 600 km with a Chapman-α function [*Rishbeth and Garriott*, 1969], following the methodology by *Lei et al.* [2005, 2007b] and *L. Liu et al.* [2007a, 2007b]:

$$\mathrm{Ne}(h) = \mathrm{NmF2} \cdot \exp[0.5 \cdot (1 - Z - \exp(-Z))],$$
$$Z = (h - \mathrm{hmF2})/\mathrm{H}(h). \quad (1)$$

We take Chapman scale height to $\mathrm{H}(h) = \mathrm{A}_1 \bullet (h - \mathrm{hmF2}) + \mathrm{Hm}$ in the bottomside, and $\mathrm{H}(h) = \mathrm{A}_2 \bullet (h - \mathrm{hmF2}) + \mathrm{Hm}$ in the topside. Thus NmF2, hmF2, Hm, A_1, and A_2 are adjustable variables, and then are determined from the electron density profile with a least squares fitting procedure. For each profile, a related coefficient and two relative mean square roots (i.e., the ratio of mean square root, between the fitted profile and data, to 20, 80 percentiles of each profile) are calculated from the above fitting. According to critical values of the related coefficient and the relative mean square roots, we discard some bad profiles, about 5% of all profiles. Then, we select those profiles collected in magnetically quiet and moderate times (Dst > -30 nT). Profiles in the ± 15 days around the equinoxes and solstices are chosen to investigate the seasonal variability. In this study, we mainly concern about the behaviors of the ionosphere at magnetic midlatitudes (dip angle about from $\pm 40^\circ$ to $\pm 70^\circ$). The magnetic inclination and declination are calculated from the 10th generation International Geomagnetic Reference Field model (IGRF-10, obtained from www.ngdc.noaa.gov/IAGA/vmod/igrf.html) at 250 km altitude.

3. Results

3.1. NmF2 Evolution on UT Map

[11] Figures 1a–1f show global snapshots of NmF2 at three UT bands (04–05, 12–13, 20–21 UT) in solstices, constructed from F3/C data. As an example to show the data coverage, Figure 1f presents an NmF2 scatterplot, which is sampled in the 20–21 UT band in December solstice. The longitude and latitude coverage is mostly complete, partic-

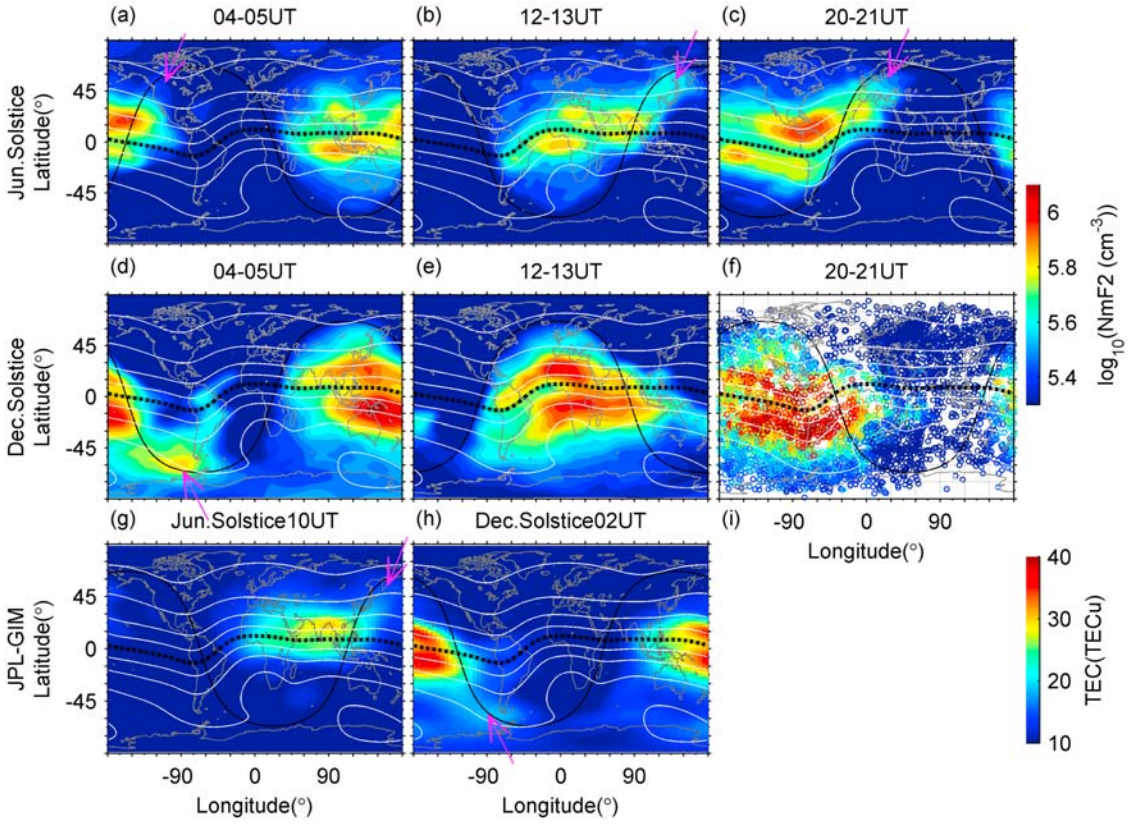

Figure 1. Global snapshots of (a–f) NmF2 (deduced from F3/C data) and (g, h) TEC (constructed from Jet Propulsion Laboratory global ionosphere map). In each panel, solid white lines are contours of dip angles with a 20° interval, the dashed line indicates the dip equator, the black solid line represents the terminator, and the magenta arrow designates the tail structure.

ularly in the dusk sector at midlatitudes. Figures 1a–1e are constructed by splitting each cell, with a resolution of 5° longitude by 2.5° latitude, into a triangle and applying a linear interpolation inside each triangle. Solid white lines illustrate contours of dip angles with a 20° interval. In Figure 1, when the ionosphere is irradiated, a pronounced double peak centers around ±20–±40° dip on either side of the magnetic dip equator (dashed curves), which is induced by the well-known fountain effect. Interestingly, at 12–13 UT in June solstice, the high value of NmF2 extend seemingly to 60–80° dip along the dusk section of the terminator (black solid lines), which is characterized by a taillike structure, denoted by the magenta arrow in Figure 1b. At the other two UT bands in June solstice, the tail could also be found, but not as distinct as that at 12–13 UT. In December solstice, the tail structure develops best at 04–05 UT (Figure 1d), but it can hardly be observed at 12–13 UT and 20–21 UT. Figure 1g shows a global mean TEC map at 10 UT in June solstices while Figure 1h shows the case at 02 UT in December solstice. These TEC plots are constructed from Jet Propulsion Laboratory global ionosphere map TEC data of 2006, 2007 and 2008. The taillike enhancement could be found in both TEC maps.

3.2. F2 Layer Evolution on LT Map

[12] To investigate the longitudinal distribution of the taillike enhancement, NmF2 shown in Figure 1 are reconstructed in three LT bands (16–17, 20–21, 21–22 LT). Figure 2 presents a series of global NmF2 maps for these LT bands in equinoxes and solstices (marked on the left axis of Figure 2). In the December solstice evening, NmF2 increases in the region around −60° dip, 30–150°W (denoted with upward arrows) [*Burns et al.*, 2008]. In the June solstice evening, NmF2 increases around 60° dip at longitudes except between 60 and 120°W (denoted with downward arrows) [*Lin et al.*, 2009; *Horvath and Lovell*, 2009b]. Furthermore, it is noteworthy that around ±60° dip where the summer enhancement appears, NmF2 increases slightly or decays slowly in the equinox evening. The southern situations in the equinoxes are consistent with TEC result in a recent study [*Jee et al.*, 2009], while this northern hemisphere, equinox phenomenon is first reported here. Coincidentally, at 20–21 LT in the March equinox, NmF2 around 60° dip is larger at locations where the declination is negative (westward), while around −60° dip, it is larger where the declination is positive (compare Figures 4d and 4h, a global map of the declination), which implies that the evening NmF2 distribution is also modulated by the magnetic declination but not uniformly between the two hemispheres.

[13] Considering that the electron density enhancement in the summer southern hemisphere is associated with the rise of F2 peak [*Burns et al.*, 2008], we constructed Figure 3 in the same way as Figure 2 but for hmF2. In June solstice, the increase of NmF2 in the northern midlatitudes also accompanies with the rise in hmF2. In addition, around ±60° dip,

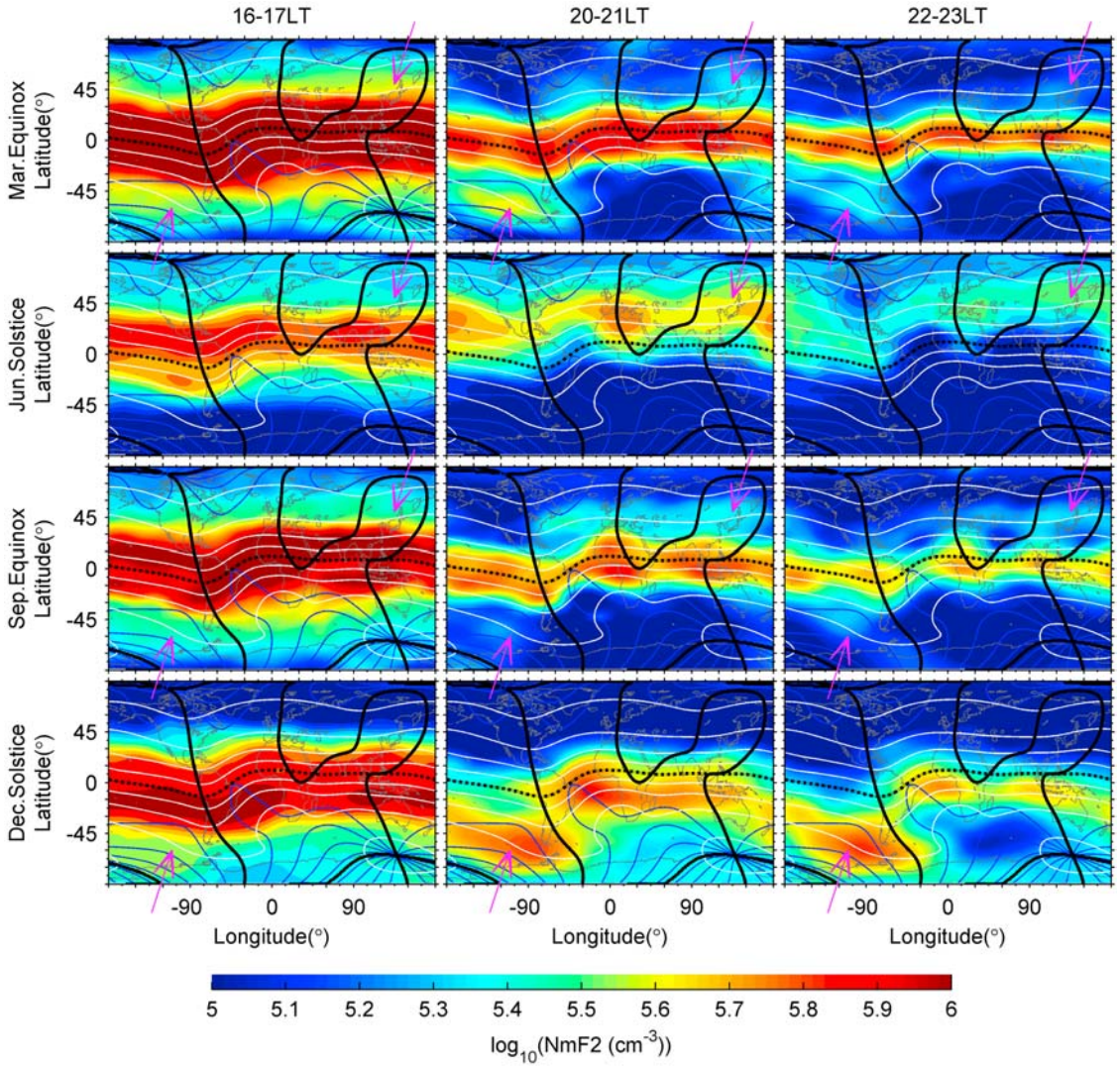

Figure 2. Global maps of NmF2 at 16–17, 20–21, 22–23 LT bands in every season, deduced from F3/C data. In each panel, the dashed line shows the dip equator, white solid lines are dip contours with a 20° interval, thick black solid lines indicate 0° declination, blue solid lines are declination contours with a 20° interval, and magenta arrows direct the regions where NmF2 is increasing or decaying slowly.

hmF2 also experiences comparable increment in the evening of the other seasons.

3.3. Distribution of Net Increases in NmF2 and hmF2

[14] Figure 4a shows a map of the increment in NmF2 from 17:00–18:30 LT to 19:00–20:30 LT in local summer (i.e., the difference between NmF2 sampled in 17:00–18:30 LT and that in 19:00–20:30 LT) in the northern hemisphere. By comparing the increment of hmF2 in series LT bands, we find that from 16:00–17:30 LT to 18:00–19:30 LT (an hour before that in Figure 4a), hmF2 increment (Figure 4b) presents a similar pattern to that in Figure 4a. In some ionospheric events, ionosonde measurements [i.e., *Prölss and Ocko*, 2000] and simulations [i.e., *Bauske and Prölss*, 1997] also represented that the response in NmF2 lagged about 2 h behind the variation in hmF2. The NmF2 does not react immediately potentially owing to the ionospheric cumulative nature [cf. *Bailey et al.*, 1997]. Figures 4c and 4d illustrate the northern geomagnetic field characters, the $|\sin(2I)|$ value (Figure 4c; I denotes the inclination) and the declination (Figure 4d). Figures 4e–4h show the corresponding distributions for the southern hemisphere.

[15] In general, the contours of hmF2 increment are roughly parallel with the contours of $|\sin(2I)|$ (e.g., most of the places with an increment more than 20 km are confined in regions with a $|\sin(2I)|$ value larger than 0.7, and those with an increment more than 5 km are mainly confined in the regions with a $|\sin(2I)|$ larger than 0.5). Exceptionally, in the southern midlatitudes, hmF2 hardly increases noticeably in the regions with a westward declination angle above 20° ($D < -20°$, in the blue line in Figure 4f). In northern midlatitudes, the absolute value of declination is mainly below 20°, and the hmF2 increment is not dependent on the declination so clearly as in the southern hemisphere. Another feature is that at the poleward side of a parallel of latitude (around 30–35° geographic latitude, consult the thick solid circles in

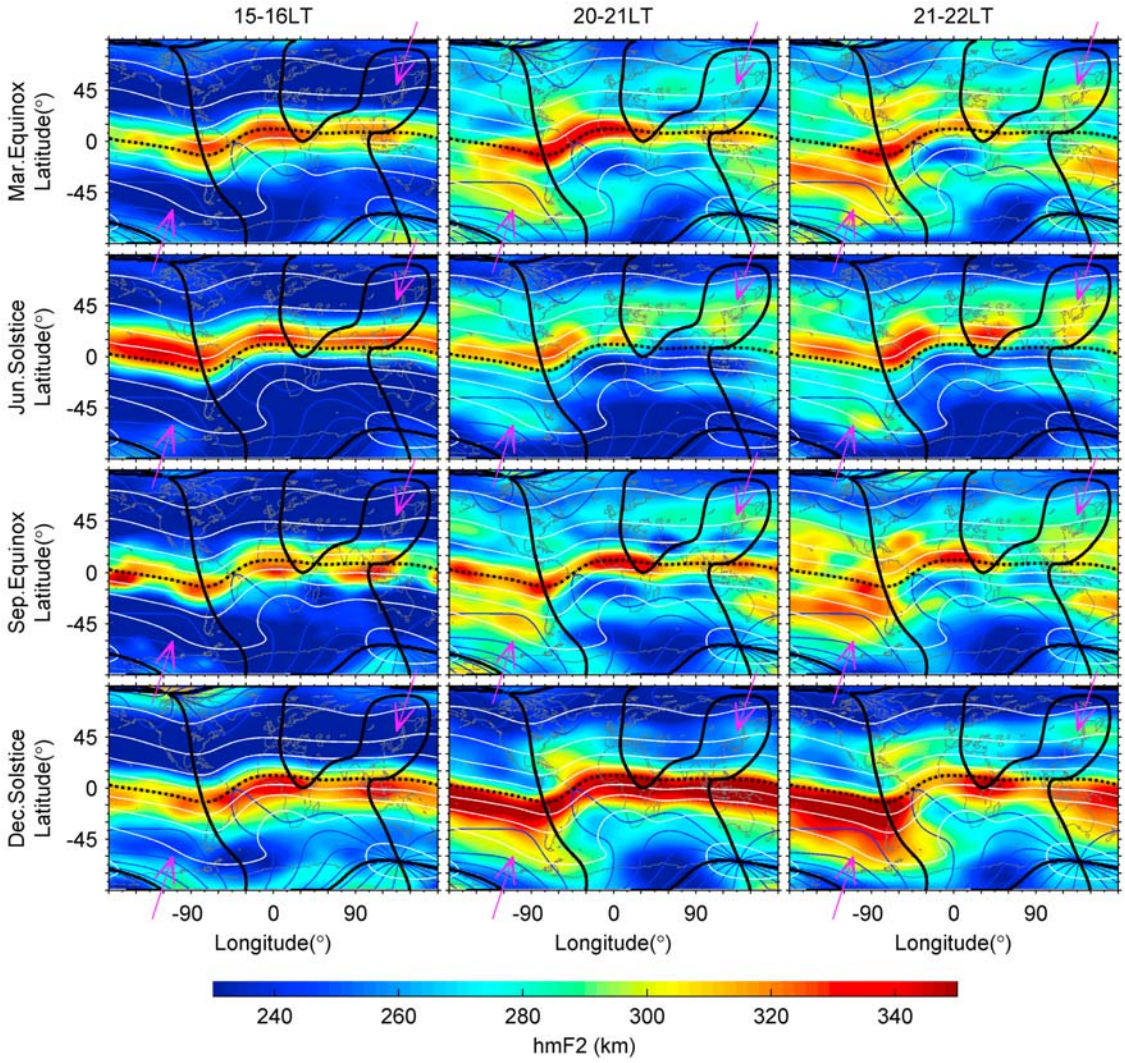

Figure 3. Same as Figure 2 but for evening hmF2.

Figures 4a–4c and 4e–4g), a greater NmF2 increment (Figures 4a and 4e) appears when hmF2 experiences a larger rise (Figures 4b and 4f). In contrast, at the equatorward side of the parallel of latitude, NmF2 hardly increases, though hmF2 has increase intensely at some locations, e.g., at 0–45°E, 15–30°S.

4. Discussion

[16] We have illustrated the evening evolutions of global NmF2 with universal time and local time, which was compared with the pattern of the magnetic field. The distinct features of the evening F2 peak enhancement are summarized as follows.

[17] 1. In local summer evening, NmF2 greatly increases in parts of dip midlatitudes. hmF2 experiences a larger increment before a stronger NmF2 enhancement.

[18] 2. In regions with the summer enhancement, NmF2 decays relatively slowly in the equinox evening, while hmF2 rises in the evening of every season.

[19] 3. The evening evolution of midlatitude F2 peak is also modulated by magnetic declination, which is not consistent in different hemispheres. These features are shown in Figures 1–4.

[20] *Oliver et al.* [2008] carried out semiquantitative estimates on the variations of hmF2 and NmF2 in the midlatitude ionosphere in response to geophysical factors. We refer the paper to readers for a detailed discussion of the behaviors of F2 peak under changes of the temperature, neutral density, thermospheric neutral wind, etc. Without considering the drift induced from winds and electric fields, hmF2 in equilibrium condition appears at altitudes above which the diffusion determines a negative density gradient, below which the chemistry processes determine a positive density gradient. hmF2 would rise under the changes that intensify the chemistry processes or weaken the diffusion. Regarding to the enhancement of F2 peak occurred over South Pacific at summer dusk, various possible physical mechanisms were considered by *Burns et al.* [2008]. We summarize simply those points here and readers are referred to the paper for full discussion. Thermal expansion could raise the F2 peak, but the atmosphere is contracting in the evening for temperatures decrease from about 15 LT. A decrease in the $[O]/[N_2]$ ratio, making the chemistry more

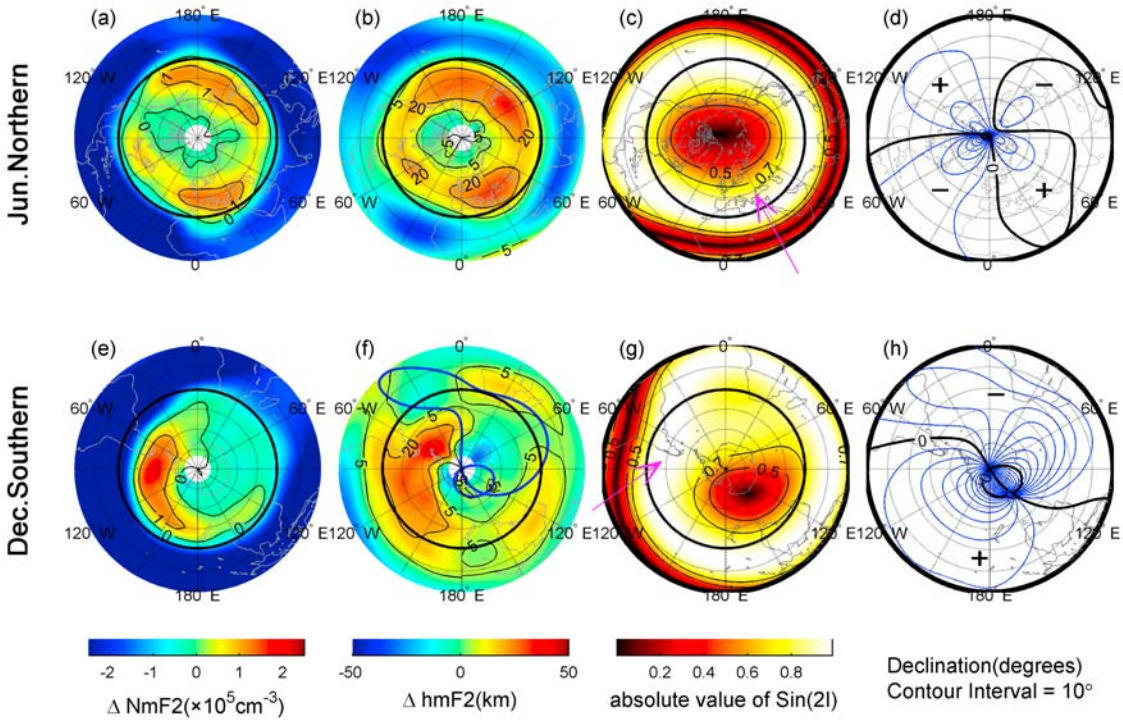

Figure 4. (a–d) Northern hemisphere maps of the increment in NmF2 (Figure 4a) from 17:00–18:30 LT to 19:00–20:30 LT in summer solstice, the increment in hmF2 (Figure 4b) from 16:00–17:30 LT to 18:00–19:30 LT in summer solstice, $|\sin(2I)|$ value (Figure 4c), and contours for magnetic declination (Figure 4d). (e–h) The cases for the southern hemisphere. The thick circles in Figures 4a–4c and 4e–4g are roughly the equatorward boundaries of the increased NmF2. The blue line in Figure 4f indicates −20° declination.

effective, could rise the F2 peak, but electron densities in the F2 region would decrease for the increased recombination. No known change of electric field that could induce such a climatology rise in hmF2 and the drifts arising from electric fields are in an inferior position on climatology comparing to those arising from winds in these dip zones. However, at dusk the prevailing wind in quiet time should be the zonal wind in general, according to the TIGCM model calculations, which would not be efficient at blowing the ionization up. Finally, *Burns et al.* [2008] proposed that contrasting with above mechanisms, the downward ambipolar diffusion, by charge exchange between the H^+ from the plasmasphere and the O atomic, may be the most possible explanation. The previous study has documented a number of mechanisms that can potentially explain the increase in hmF2. Apart from the comprehensive discussion by *Burns et al.* [2008], we suggest that the thermospheric winds mechanism (in stead of the diffusion mechanism) should be the most potential concern with regards to our results for a number of reasons. First, during the period of the plasma transported from the plasmasphere, TEC should not increase significantly, however remarkable TEC increases were observed by TOPEX [*Horvath*, 2006]. Second, the diffusion mechanism is insufficient to explain the distinct declination dependences of the evening F2 peak properties. It also cannot explain that the NmF2 enhancement ends short around local sunset (it will be showed in section 4.2). Third, according to observations and the horizontal wind model, the equatorward winds would appear around or before 15 LT at midlatitudes in summer, earlier than other seasons [*Foppiano et al.*, 2003; *Kawamura et al.*, 2000; *Lei et al.*, 2007a]. Fourth, the increasing hmF2 need not appear with an equatorward flow, whereas it can occur with the poleward winds receding from its maximum (a detail discussion is contained in section 4.1).

4.1. Thermospheric Wind Effect

[21] The behavior of the F2 peak is controlled by the combined effect of the production and loss of ionization as well as by transport processes. In the absence of any vertical drift, the equilibrium F2 peak will appear at h_b with a peak density N_b, where the time constants for the linear chemical loss and plasma diffusion are similar. When a downward or upward drift (V_z) presents, hmF2 will decrease or increase, which would not continue indefinitely, and the F2 peak would finally form at a new height h_{bw}, as in the servo manner [*Rishbeth*, 1967, 1968]. The ratio of $(h_{bw}-h_b)/V_z$ changes with location, local time and other factors, and the order of magnitude of this ratio is around 1 km/(m/s) [*Miller et al.*, 1986; *Oliver et al.*, 2008; *Richards*, 1991]. During the daylight hours, the equilibrium NmF2 is approximately proportional to the ratio $[O]/[N_2]$ when an equilibrium altitude of F2 peak is established. The ratio $[O]/[N_2]$ increases with altitude as $\exp(\Delta h \bullet (1/H_{N2}-1/H_O))$, H_O and H_{N2} are scale height of O and N_2. Assuming H_O and H_{N2} are irrelevant to height here for a rough estimation, the drift equilibrium peak density $N_{bw} = N_b \bullet \exp(C \bullet (h_{bw}-h_b))$, C is a positive constant.

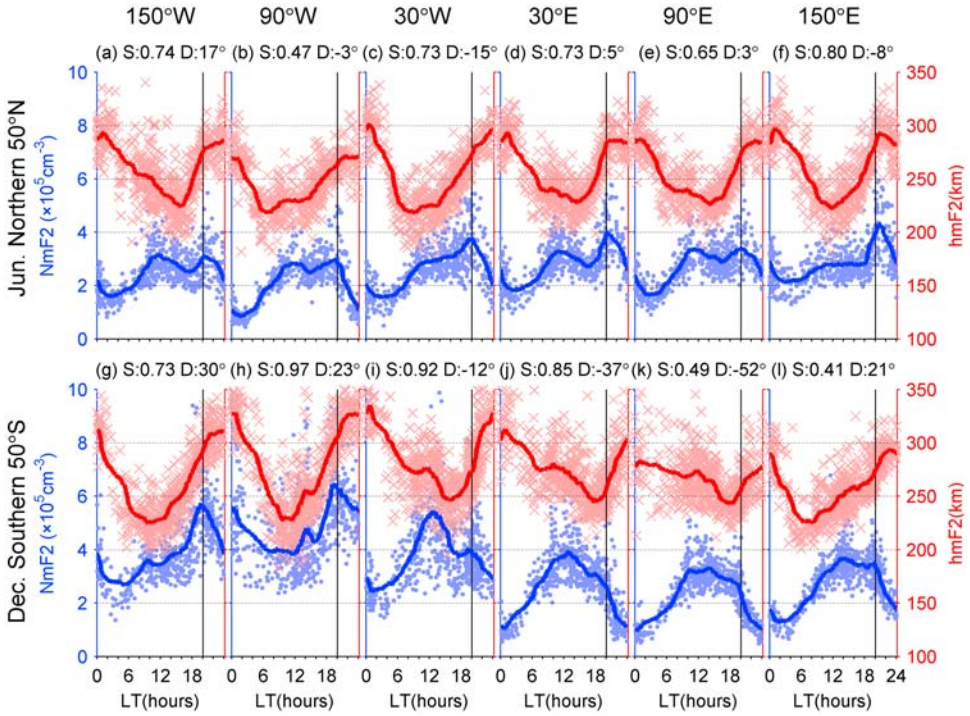

Figure 5. (a–f) Diurnal variations of the NmF2 (blue points and their moving average) and hmF2 (red crosses and their moving average) at 50°N and six longitude sectors, i.e., 150°W, 90°W, 30°W, 30°E, 90°E and 150°E in local summer solstice. (g–l) The cases at 50°S. In the title of each panel, the character "S" denotes the value of $|\sin(2I)|$ and "D" denotes the declination; the black line indicates the LT moment of the local sunset.

[22] The drift could be caused by either electric fields or horizontal winds. In the F region, the effective upward drift velocities of plasma induced by an eastward electric field E_y in geomagnetic field **B**, and by the wind of magnitude U with an azimuth θ are:

$$V_z = (E_y/B) \cdot \cos(I) \tag{2a}$$

$$V_z = -U/2 \cdot \sin(2I) \cdot \cos(\theta - D) \tag{2b}$$

Here I is the magnetic dip angle, and D is the magnetic declination [e.g., *Dudeney and Piggott*, 1978; *Horvath*, 2006; *Rishbeth*, 1967, 1972, 1998; *Rishbeth and Kelley*, 1971].

[23] The horizontal winds are most effective at blowing the ionization vertically at dip midlatitudes for the large value of $\sin(2I)$. The magnitude of E_y-induced drifts is on climatology a small fraction of the magnitude of wind-induced drifts at dip midlatitudes [e.g., *Kawamura et al.*, 2002; *Oliver et al.*, 2008]. Taking just the winds into account, the increase in h_{bw} and N_{bw}, as suggested by the above analysis, is occurring in the periods with either enhancing equatorward winds or weakening poleward winds. In the latter situation, the increases in hmF2 and NmF2 occur as recovering to h_b and N_b, a potential result of which is that the increases of hmF2 and NmF2 could set in at 12–14 LT (as in Figures 5c, 5g, and 5h), though the equatorward wind may appear as late as 15 LT. Figure 5 shows the diurnal variations of NmF2 (the blue scattered points and their running average) and hmF2 (the red symbols) in six longitude sectors at 50°N and 50°S latitude in local summer, with a resolution of 20° longitude by 10° latitude. The agreement between similar curves of F3/C and ionosonde observations was illustrated in Figure 3 of *Luan et al.* [2008].

4.2. Longitudinal Difference of Diurnal F2 Peak Variation

[24] In Figure 5, hmF2 increases from their diurnal minimum at daytime, and reaches the maximum at night. This characteristic of midlatitude hmF2 is induced qualitatively by the winds [*Rishbeth*, 1968; *Su et al.*, 1997]. Clearly, there are distinct longitude differences of the morphologies of diurnal hmF2 and NmF2.

[25] According to equation (2b), the vertical plasma drift induced by winds is dependent on the components (D and I) of the magnetic field. So the diurnal variation of hmF2 is closely related to the geometry of the magnetic field. In the midlatitude F region, the zonal prevailing winds are mainly westward before dawn and eastward after dusk; the meridional prevailing winds are mainly poleward during daytime and equatorward during nighttime [cf. *Emmert et al.*, 2003, 2006; *Hedin et al.*, 1988, 1991; *Titheridge*, 1995; *Wu et al.*, 1994]. It is implied that the azimuth θ rotates through 360° in the diurnal 24 h and the value of $\cos(\theta\text{-D})$ changes between −1 to 1 [also cf. *Rishbeth and Kelley*, 1971]. In the southern midlatitudes, θ decreases roughly from about 270° to 90° in the daytime. In this period, the downward maximum V_z (when $\partial V_z/\partial\theta = 0$, i.e., $\sin(\theta - D) = 0$ or $\theta - D = 180°$ here) tends to occur earlier if the declination is positive (eastward). Accordingly, in longitudes with a positive declination (Figures 5g, 5h, and 5l), the diurnal main valley of hmF2

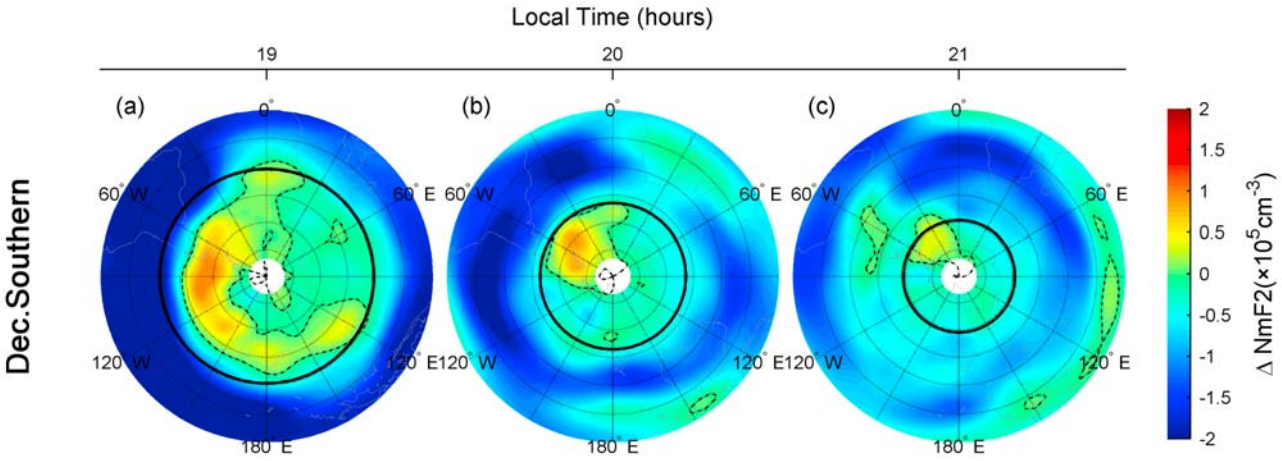

Figure 6. (a–c) Southern hemisphere maps of an hour increment in NmF2 around 19, 20, and 21 LT in December solstice. For example, Figure 6a is the difference between NmF2 sampled in 19–20 LT and that in 18–19 LT. In each panel, the thick circle indicates the terminator at corresponding LT moment; dashed lines are the boundaries of regions with a positive increment of NmF2.

appears mainly in the morning; otherwise, in the longitude with a westward declination (Figures 5i, 5j, and 5k), the main valley of hmF2 appears in the afternoon. In the northern midlatitudes, the downward maximum V_z appears also when $\partial V_z/\partial\theta$ reaches 0 (i.e., $\sin(\theta-\mathrm{D}) = 0$ here). However, different from the southern midlatitudes, the azimuth θ increases (from about 270° to 360° then to about 90°) during the daytime, so that the downward maximum V_z occurs earlier when the declination is negative (westward). Consequently, in the longitude with a negative declination (Figure 5a), the main valley of hmF2 appears earlier than that with a positive declination (Figure 5c). Around dusk, the declination dependence of hmF2 is difference in the two hemispheres, for that the graphic eastward wind would drift the ionization upward where the declination is eastward in the southern hemisphere but downward in the northern hemisphere. Besides, horizontal winds would be more effective at drifting the ionization vertically when the $|\sin(2I)|$ value is larger. The diurnal amplitude of hmF2 would be larger if the $|\sin(2I)|$ value is larger, as indicated in Figure 5. In conclusion, the diurnal amplitude and phase of hmF2 clearly depend on the inclination and declination respectively. Thus, the pattern of the magnetic field could induce the pattern of the evening evolution of hmF2 in Figures 4b and 4f.

[26] The NmF2 generally peaks in two LT bands, around noon (10–14 LT) and ground sunset (Figure 5). In the northern hemisphere (Figures 5a–5f), the maximal peak of NmF2 is usually the sunset peak; the longitudinal variation, of the difference between the noon peak and the sunset, is indistinctive compared with that in the southern hemisphere. In the southern hemisphere, the sunset peak is extraordinarily prominent at 90–150°W, but can hardly be observed at 30–90°E. Rough calculations showed that in midlatitudes an evening increase of NmF2 may occur in summer but is sensitive to details of the winds [*Rishbeth*, 1967, 1968]. *Su et al.* [1997] published comparative modeling studies of the effects arising from the wind and drift on the diurnal variation of the electron density profile upon observations of the middle and upper atmosphere (MU) radar, at Shigaraki (34.9°N, 136.1°E, dip 49.1°, apex latitude 27.7°), Japan. Su et al. concluded that the thermospheric wind is responsible for the observed feature that the electron density is lower at noon than that at sunset. Despite building upon the MU Radar observations, results of *Su et al.* [1997] can act as an important reference for understanding the broadly midlatitude ionosphere. In Figure 5, various morphologies of the NmF2 curves are potentially resulted from the competition of the effects arising from the wind changing (hinted by the trend of hmF2) with the decreasing production caused by the sun falling. When hmF2 reaches its main valley in the morning and keeps a low height to afternoon, the noon NmF2 peak may not exist (Figures 5c, 5f, and 5g). When hmF2 falls to its main valley after noon and then rises quickly, a corresponding valley may be impressed in the NmF2 curve (Figures 5a, 5d, and 5i). Besides, the sunset plays a key role in shaping the evening NmF2. Similar to the situation in calculations of *Su et al.* [1997], the increases of NmF2 in Figure 5 stop around the local sunset. Actually, the thick circles in Figures 4a–4c and Figures 4e–4g (i.e., the equatorward boundaries of the increased NmF2) overlaps roughly with the terminator line (31° latitude at 19 LT). It is worth noting that the above results are for the equatorward edge of the Weddell Sea zone. Larger part of the special WSA appears at higher latitudes accompanied by the polar day. The same plot as in Figure 5 but for the Weddell Sea region (20° longitude by 10° latitude around 37°W, 67.5°S), which is not presented in this paper, shows that the enhancement of NmF2 there continues to the middle of the night.

[27] The evening evolutions of midlatitude hmF2 are similar in different seasons for the azimuth θ changes roughly in the similar way [also cf. *Lei et al.*, 2005]. The diurnal maximum poleward wind and the equatorward wind appear earlier in summer than other seasons (especially than winter) [e.g., *Foppiano et al.*, 2003], then the afternoon rise of F2 peak occurs earlier in summer (Figure 3) than in winter. But, at 45–65° latitude, local sunset occurs earlier by about 2–4 h or 4–8 h in equinoxes or winter, compared with that in summer solstice. Accordingly, NmF2 dose not

increase persistently in equinox evening as that in local summer solstice (Figure 2), let alone winter. More detailed discussion about the equinox cases was provided by *Jee et al.* [2009].

4.3. Characteristics of Southern Enhancement

[28] Compared with the NmF2 enhancement in the northern hemisphere, the southern WSA is characterized by distinct zonal asymmetry as well as greater increment in NmF2 and hmF2. The pattern of the southern magnetic field is extraordinarily asymmetrical zonally because the south magnetic pole departures severely from the geographic pole. In longitude sectors far from the magnetic pole (30–120°W), the southern magnetic midlatitude occurs at comparatively higher geographic latitude, e.g., the highest geographic latitude on contour of $-60°$ dip is about 68°S around the Weddell Sea. The local sunset occurs later and the incident solar radiation declines more slowly at higher geographic latitude. Then, the NmF2 enhancement would persist to late night over there. Figure 6 illustrates a southern hemisphere map series of an hour increment in NmF2 around 19, 20, 21 LT in the December solstice (e.g., Figure 6a shows the difference between NmF2 sampled in 19–20 LT and that in 18–19 LT). The equatorward boundary, of the regions with a positive increment of NmF2 (contained in dashed lines), is shrinking gradually toward the geographic pole from 19 LT to 21 LT, accompanied by the shrinking terminator (thick circle). The increasing NmF2 is mostly confined to the Weddell Sea zone at 21 LT.

[29] At 90°W, 50°S (Figure 5h), the $|\sin(2I)|$ value is 0.97 and the magnetic declination is about 23°. Then the diurnal amplitude of hmF2 is large, and the main valley of hmF2 appears around noon. From noon to sunset, hmF2 rises rapidly from 225 km to 300 km and NmF2 increases from 4×10^5 cm^{-3} to 6.5×10^5 cm^{-3}. Consequently, in the evening of the southern summer solstice, NmF2 maximizes over there (right bottom panel in Figure 2).

5. Conclusions

[30] The peak electron density and peak height of the F2 layer are extracted from a large number of F3/C IRO electron density profiles. These data are utilized to analyze the evolution of the general WSA in difference seasons and its longitude variation, and to compare the obtained results with the special WSA. The F2 layer behaviors at midlatitudes are found to be associated with the geometry of the magnetic field. Our major findings are as follows.

[31] 1. In local summer evening, NmF2 greatly enhances in some regions of dip midlatitudes. In regions appearing the summer enhancement, NmF2 decays relatively slowly or increases slightly in the evening of equinoxes, comparing to other regions.

[32] 2. In the evening, the magnetic declination dependence of NmF2 is opposite between the two hemispheres. The NmF2 is generally higher where the magnetic declination is eastward in the southern hemisphere but westward in the northern hemisphere, albeit it is less characteristic in the northern hemisphere where the longitudes difference of the declination is less significant than in the southern hemisphere.

[33] 3. A greater increment in hmF2 occurs before the stronger NmF2 enhancement. Comparable variation in hmF2 also appears there in the evening of equinoxes and winter.

[34] 4. The increase of NmF2 terminates around the local sunset, indicating the significant contribution of the local solar produced ionization in supplying the plasma.

[35] The general WSA appearing in both hemispheres accords well with the above behaviors, all of which could be appropriately explained in terms of the evolution of thermospheric neutral winds and the geometry of the magnetic field.

[36] 1. Upward (downward) ionization drifts would increase (decrease) the F2 peak height. The wind-induced vertical drift depends on the wind components as well as the magnetic components. At midlatitudes, the diurnal variation of hmF2 is affected qualitatively by the diurnal changing of winds. Meanwhile the diurnal amplitude of hmF2 depends on the magnetic inclination, and the diurnal phase of hmF2 relies on the magnetic declination.

[37] 2. Generally, hmF2 is increasing in the evening of all seasons, details of which are sensitive to the magnetic components and the wind changing. The increase in hmF2 occurs early where the declination is eastward in southern hemisphere but westward in northern hemisphere.

[38] 3. If hmF2 experiences a considerable increase before the local sunset, an increase in NmF2 could be induced. In local summer the sun sets later at higher latitudes. The increase in NmF2 ends at its latest near the Weddell Sea zone and the evening NmF2 maximizes at 90°W, 50–60°S due to their particular geographical positions with special geometries of the magnetic field.

[39] Based on the results above, we suggest the thermospheric wind mechanism may be the most potential explanation, which needs further modeling.

[40] **Acknowledgments.** We thank Jiuhou Lei for his constructive suggestions and Kunjie Wen, Keyan Fang for their helps in the literature. This study made use of the IRO data from the COSMIC Data Analysis and Archive Center. This work was supported by the National Natural Science Foundation of China (40725014, 40674090, 40636032) and National Important Basic Research Project (2006CB806306).

[41] Zuyin Pu thanks Alan Burns and another reviewer for their assistance in evaluating this paper.

References

Bailey, G. J., N. Balan, and Y. Z. Su (1997), The Sheffield University plasmasphere ionosphere model—A review, *J. Atmos. Sol. Terr. Phys.*, *59*(13), 1541–1552, doi:10.1016/S1364-6826(96)00155-1.

Bauske, R., and G. W. Prölss (1997), Modeling the ionospheric response to traveling atmospheric disturbances, *J. Geophys. Res.*, *102*(A7), 14,555–14,562, doi:10.1029/97JA00941.

Bellchambers, W., and W. Piggott (1958), Ionospheric measurements made at Halley Bay, *Nature*, *182*(4649), 1596–1597, doi:10.1038/1821596a0.

Burns, A. G., Z. Zeng, W. Wang, J. Lei, S. C. Solomon, A. D. Richmond, T. L. Killeen, and Y.-H. Kuo (2008), Behavior of the F_2 peak ionosphere over the South Pacific at dusk during quiet summer conditions from COSMIC data, *J. Geophys. Res.*, *113*, A12305, doi:10.1029/2008JA013308.

Chan, K., and L. Colin (1969), Global electron density distributions from topside soundings, *Proc. IEEE*, *57*(6), 990–1004, doi:10.1109/PROC.1969.7143.

Dickinson, R. E., E. C. Ridley, and R. G. Roble (1981), A three-dimensional general circulation model of the thermosphere, *J. Geophys. Res.*, *86*(A3), 1499–1512, doi:10.1029/JA086iA03p01499.

Dudeney, J. R., and W. R. Piggott (1978), Antarctic ionospheric research, in *Upper Atmosphere Research in Antarctica*, *Antarct. Res. Ser.*, vol. 29, edited by L. J. Lanzerotti and C. G. Park, pp. 200–235, AGU, Washington, D. C.

Emmert, J. T., B. G. Fejer, and D. P. Sipler (2003), Climatology and latitudinal gradients of quiet time thermospheric neutral winds over Millstone Hill from Fabry-Perot interferometer measurements, *J. Geophys. Res.*, *108*(A5), 1196, doi:10.1029/2002JA009765.

Emmert, J. T., M. L. Faivre, G. Hernandez, M. J. Jarvis, J. W. Meriwether, R. J. Niciejewski, D. P. Sipler, and C. A. Tepley (2006), Climatologies of nighttime upper thermospheric winds measured by ground-based Fabry-Perot interferometers during geomagnetically quiet conditions: 1. Local time, latitudinal, seasonal, and solar cycle dependence, *J. Geophys. Res.*, *111*, A12302, doi:10.1029/2006JA011948.

Foppiano, A. J., X. A. Torres, M. A. Arriagada, and P. A. Flores (2003), Meridional thermospheric winds over the Antarctic Peninsula longitude sector, *J. Atmos. Sol. Terr. Phys.*, *65*(3), 305–314, doi:10.1016/S1364-6826(02)00287-0.

Hedin, A. E., N. W. Spencer, and T. L. Killeen (1988), Empirical global model of upper thermosphere winds based on Atmosphere and Dynamics Explorer satellite data, *J. Geophys. Res.*, *93*(A9), 9959–9978.

Hedin, A. E., et al. (1991), Revised global model of thermosphere winds using satellite and ground-based observations, *J. Geophys. Res.*, *96*(A5), 7657–7688, doi:10.1029/91JA00251.

Horvath, I. (2006), A total electron content space weather study of the nighttime Weddell Sea Anomaly of 1996/1997 southern summer with TOPEX/Poseidon radar altimetry, *J. Geophys. Res.*, *111*, A12317, doi:10.1029/2006JA011679.

Horvath, I. (2007), Impact of 10 January 1997 geomagnetic storm on the nighttime Weddell Sea Anomaly: A study utilizing data provided by the TOPEX/Poseidon mission and the Defense Meteorological Satellite Program, and simulations generated by the Coupled Thermosphere/Ionosphere Plasmasphere model, *J. Geophys. Res.*, *112*, A06329, doi:10.1029/2006JA012153.

Horvath, I., and E. A. Essex (2003), The Weddell Sea Anomaly observed with the Topex satellite data, *J. Atmos. Sol. Terr. Phys.*, *65*(6), 693–706, doi:10.1016/S1364-6826(03)00083-X.

Horvath, I., and B. C. Lovell (2009a), Investigating the relationships among the South Atlantic Magnetic Anomaly, southern nighttime midlatitude trough, and nighttime Weddell Sea Anomaly during southern summer, *J. Geophys. Res.*, *114*, A02306, doi:10.1029/2008JA013719.

Horvath, I., and B. C. Lovell (2009b), An investigation of the northern hemisphere midlatitude nighttime plasma density enhancements and their relations to the midlatitude nighttime trough during summer, *J. Geophys. Res.*, *114*, A08308, doi:10.1029/2009JA014094.

Ivanov-Kholodny, G. S., and A. V. Mikhailov (1986), *The Prediction of Ionospheric Conditions*, D. Reidel, Dordrecht, Netherlands.

Jee, G., A. G. Burns, Y.-H. Kim, and W. Wang (2009), Seasonal and solar activity variations of the Weddell Sea Anomaly observed in the TOPEX total electron content measurements, *J. Geophys. Res.*, *114*, A04307, doi:10.1029/2008JA013801.

Kawamura, S., Y. Otsuka, S.-R. Zhang, S. Fukao, and W. L. Oliver (2000), A climatology of middle and upper atmosphere radar observations of thermospheric winds, *J. Geophys. Res.*, *105*(A6), 12,777–12,788.

Kawamura, S., N. Balan, Y. Otsuka, and S. Fukao (2002), Annual and semiannual variations of the midlatitude ionosphere under low solar activity, *J. Geophys. Res.*, *107*(A8), 1166, doi:10.1029/2001JA000267.

Lei, J., L. Liu, W. Wan, and S.-R. Zhang (2005), Variations of electron density based on long-term incoherent scatter radar and ionosonde measurements over Millstone Hill, *Radio Sci.*, *40*, RS2008, doi:10.1029/2004RS003106.

Lei, J., R. G. Roble, S. Kawamura, and S. Fukao (2007a), A simulation study of thermospheric neutral winds over the MU radar, *J. Geophys. Res.*, *112*, A04303, doi:10.1029/2006JA012038.

Lei, J., et al. (2007b), Comparison of COSMIC ionospheric measurements with ground-based observations and model predictions: Preliminary results, *J. Geophys. Res.*, *112*, A07308, doi:10.1029/2006JA012240.

Lin, C. H., J. Y. Liu, C. Z. Cheng, C. H. Chen, C. H. Liu, W. Wang, A. G. Burns, and J. Lei (2009), Three-dimensional ionospheric electron density structure of the Weddell Sea Anomaly, *J. Geophys. Res.*, *114*, A02312, doi:10.1029/2008JA013455.

Liu, H., C. Stolle, S. Watanabe, T. Abe, M. Rother, and D. Cooke (2007), Evaluation of the IRI model using CHAMP observations in polar and equatorial regions, *Adv. Space Res.*, *39*(5), 904–909, doi:10.1016/j.asr.2006.08.006.

Liu, L., H. Le, W. Wan, M. P. Sulzer, J. Lei, and M.-L. Zhang (2007a), An analysis of the scale heights in the lower topside ionosphere based on the Arecibo incoherent scatter radar measurements, *J. Geophys. Res.*, *112*, A06307, doi:10.1029/2007JA012250.

Liu, L., W. Wan, M. Zhang, B. Ning, S. Zhang, and J. Holt (2007b), Variations of topside ionospheric scale heights over Millstone Hill during the 30-day incoherent scatter radar experiment, *Ann. Geophys.*, *25*, 2019–2027.

Liu, L., M. He, W. Wan, and M.-L. Zhang (2008), Topside ionospheric scale heights retrieved from Constellation Observing System for Meteorology, Ionosphere, and Climate radio occultation measurements, *J. Geophys. Res.*, *113*, A10304, doi:10.1029/2008JA013490.

Liu, L., B. Zhao, W. Wan, B. Ning, M.-L. Zhang, and M. He (2009), Seasonal variations of the ionospheric electron densities retrieved from Constellation Observing System for Meteorology, Ionosphere, and Climate mission radio occultation measurements, *J. Geophys. Res.*, *114*, A02302, doi:10.1029/2008JA013819.

Luan, X., and S. C. Solomon (2008), Meridional winds derived from COSMIC radio occultation measurements, *J. Geophys. Res.*, *113*, A08302, doi:10.1029/2008JA013089.

Luan, X., W. Wang, A. Burns, S. C. Solomon, and J. Lei (2008), Midlatitude nighttime enhancement in *F* region electron density from global COSMIC measurements under solar minimum winter condition, *J. Geophys. Res.*, *113*, A09319, doi:10.1029/2008JA013063.

Miller, K. L., D. G. Torr, and P. G. Richards (1986), Meridional winds in the thermosphere derived from measurement of F_2 layer height, *J. Geophys. Res.*, *91*(A4), 4531–4535, doi:10.1029/JA091iA04p04531.

Oliver, W. L., S. Kawamura, and S. Fukao (2008), The causes of midlatitude *F* layer behavior, *J. Geophys. Res.*, *113*, A08310, doi:10.1029/2007JA012590.

Penndorf, R. (1965), The average ionospheric conditions over the Antarctic, in *Geomagnetism and Aeronomy*, *Antarct. Res. Ser.*, vol. 4, edited by A. H. Waynick, pp. 1–45, AGU, Washington, D. C.

Prölss, G. W., and M. Ocko (2000), Propagation of upper atmospheric storm effects towards lower latitudes, *Adv. Space Res.*, *26*(1), 131–135, doi:10.1016/S0273-1177(99)01039-X.

Rastogi, R. G. (1960), Abnormal features of the F_2 region of the ionosphere at some southern high-latitude stations, *J. Geophys. Res.*, *65*, 585–592, doi:10.1029/JZ065i002p00585.

Richards, P. G. (1991), An improved algorithm for determining neutral winds from the height of the F_2 peak electron density, *J. Geophys. Res.*, *96*(A10), 17,839–17,846.

Rishbeth, H. (1967), The effect of winds on the ionospheric F_2-peak, *J. Atmos. Terr. Phys.*, *29*, 225–238, doi:10.1016/0021-9169(67)90192-4.

Rishbeth, H. (1968), The effect of winds on the ionospheric F_2-peak—II, *J. Atmos. Terr. Phys.*, *30*, 63–71, doi:10.1016/0021-9169(68)90041-X.

Rishbeth, H. (1972), Thermospheric winds and the *F* region: A review, *J. Atmos. Terr. Phys.*, *34*, 1–47.

Rishbeth, H. (1998), How the thermospheric circulation affects the ionospheric F_2-layer, *J. Atmos. Sol. Terr. Phys.*, *60*(14), 1385–1402, doi:10.1016/S1364-6826(98)00062-5.

Rishbeth, H., and O. K. Garriott (1969), *Introduction to Ionospheric Physics*, Academic, New York.

Rishbeth, H., and D. Kelley (1971), Maps of the vertical *F*-layer drifts caused by horizontal winds at mid-latitudes, *J. Atmos. Terr. Phys.*, *33*, 539–545, doi:10.1016/0021-9169(71)90056-0.

Rishbeth, H., and C. Kervin (1968), Seasonal changes displayed by F_1-layer ionograms, *J. Atmos. Terr. Phys.*, *30*, 1657–1665, doi:10.1016/0021-9169(68)90014-7.

Rishbeth, H., and M. Mendillo (2001), Patterns of F_2-layer variability, *J. Atmos. Sol. Terr. Phys.*, *63*(15), 1661–1680, doi:10.1016/S1364-6826(01)00036-0.

Rocken, C., Y.-H. Kuo, W. S. Schreiner, D. Hunt, S. Sokolovskiy, and C. McCormick (2000), COSMIC system description, *Terr. Atmos. Ocean Sci.*, *11*(1), 21–52.

Schreiner, W., C. Rocken, S. Sokolovskiy, S. Syndergaard, and D. Hunt (2007), Estimates of the precision of GPS radio occultations from the COSMIC/FORMOSAT-3 mission, *Geophys. Res. Lett.*, *34*, L04808, doi:10.1029/2006GL027557.

Su, Y. Z., S. Fukao, and G. J. Bailey (1997), Modeling studies of the middle and upper atmosphere radar observations of the ionospheric *F* layer, *J. Geophys. Res.*, *102*(A1), 319–327.

Titheridge, J. E. (1995), Winds in the ionosphere—A review, *J. Atmos. Terr. Phys.*, *57*(14), 1681–1714.

Wu, Q., T. L. Killeen, and N. W. Spencer (1994), Dynamics Explorer 2 observations of equatorial thermospheric winds and temperatures: Local time and longitudinal dependences, *J. Geophys. Res.*, *99*(A4), 6277–6288, doi:10.1029/93JA02521.

Zeng, Z., A. Burns, W. Wang, J. Lei, S. Solomon, S. Syndergaard, L. Qian, and Y.-H. Kuo (2008), Ionospheric annual asymmetry observed by the COSMIC radio occultation measurements and simulated by the TIEGCM, *J. Geophys. Res.*, *113*, A07305, doi:10.1029/2007JA012897.

M. He, H. Le, L. Liu, B. Ning, W. Wan, J. Wen, X. Yue, and B. Zhao, Beijing National Observatory of Space Environment, Institute of Geology and Geophysics, Chinese Academy of Sciences, Beijing 100029, China. (liul@mail.iggcas.ac.cn)